Remote Sensing of Environment 224 (2019) 401–411

Contents lists available at ScienceDirect

Remote Sensing of Environment

journal homepage: www.elsevier.com/locate/rse

A simple self-adjusting model for correcting the blooming effects in DMSP-OLS nighttime light images

Xin Cao[a], Yang Hu[a], Xiaolin Zhu[b,*], Feng Shi[c], Li Zhuo[d], Jin Chen[a]

[a] State Key Laboratory of Earth Surface Processes and Resource Ecology, Faculty of Geographical Science, Beijing Normal University, Beijing 100875, China
[b] Department of Land Surveying and Geo-Informatics, The Hong Kong Polytechnic University, Hong Kong, China
[c] Institute of Science and Technology for Development of Shandong, Qilu University of Technology (Shandong Academy of Science), Jinan 250014, China
[d] Guangdong Provincial Key Laboratory of Urbanization and Geo-simulation & Center of Integrated Geographic Information Analysis, School of Geography and Planning, Sun Yat-sen University, Guangzhou, Guangdong 510275, China

ARTICLE INFO

Keywords:
DMSP-OLS
Nighttime light
Blooming
Spatial response function
Self-adjusting model

ABSTRACT

Night-time light (NTL) data from the Defense Meteorological Satellite Program (DMSP) Operation Linescan System (OLS) provide important observations of human activities; however, DMSP-OLS NTL data suffer from problems such as saturation and blooming. This research developed a self-adjusting model (SEAM) to correct blooming effects in DMSP-OLS NTL data based on a spatial response function and without using any ancillary data. By assuming that the pixels adjacent to the background contain no lights (i.e., pseudo light pixels, PLPs), the blooming effect intensity, a parameter in the SEAM model, can be estimated by pixel-based regression using PLPs and their neighboring light sources. SEAM was applied to all of China, and its performance was assessed for twelve cities with different population sizes. The results show that SEAM can largely reduce the blooming effect in the original DMSP-OLS dataset and enhance its quality. The images after blooming effect correction have higher spatial similarity with Suomi National Polar-orbiting Partnership Visible Infrared Imaging Radiometer Suite (VIIRS) images and higher spatial variability than the original DMSP-OLS data. We also found that the average effective blooming distance is approximately 3.5 km in China, which may be amplified if the city is surrounded by water surfaces, and that the blooming effect intensity is positively correlated to atmospheric quality. The effectiveness of the proposed model will improve the capacity of DMSP-OLS images for mapping the urban extent and modeling socioeconomic parameters.

1. Introduction

Night-time light (NTL) data records nocturnal artificial light on the Earth's surface and provides unique observations for human activities (Elvidge et al., 1997a; Elvidge et al., 2001). Two main datasets that offer global coverage are available for NTL information, the digital archive of annual composite images since 1992 from the Operational Linescan System (OLS) instrument onboard Defense Meteorological Satellite Program (DMSP) satellite and nighttime light images from the Visible Infrared Imaging Radiometer Suite (VIIRS) instrument onboard the Suomi National Polar-orbiting Partnership (Suomi-NPP) satellite launched in 2011 (Bennett and Smith, 2017; Elvidge et al., 2017). In recent decades, NTL data have been widely used in socioeconomic and environmental research, including urbanization delineation and spatial distribution analyses (Small et al., 2005; Cao et al., 2009; Zhou et al., 2014; Letu et al., 2015; Xie and Weng, 2017), economic development or decline monitoring (Elvidge et al., 1997a; Henderson et al., 2012; Rohner et al., 2013), population density mapping (Zhuo et al., 2009; Townsend and Bruce, 2010), electricity consumption modeling (Lo, 2002; Letu et al., 2010; Townsend and Bruce, 2010; Cao et al., 2014; Proville et al., 2017), environmental issues such as light pollution (Cinzano et al., 2001; Longcore and Rich, 2004; Butt, 2012; Rodrigues et al., 2012; Falchi et al., 2016), air quality (Wang et al., 2016) and CO_2 emissions (Zhang et al., 2017; Proville et al., 2017).

DMSP-OLS provides the longest observations of NTL information, from 1992 to 2013, an unparalleled dataset for studying historical artificial lights; however, it suffers from four main problems: coarse spatial resolution, lack of onboard calibration, saturation and blooming (Imhoff et al., 1997; Small et al., 2011; Small et al., 2005; Elvidge et al., 2007; Bennett and Smith, 2017). The spatial resolution of DMSP-OLS data is 2.7 km, whereas NPP-VIIRS offers a finer resolution of 742 m (Bennett and Smith, 2017). DMSP-OLS NTL annual composite data available from 1992 to 2013 were acquired by sensors onboard six different satellites without onboard calibration mechanisms (Elvidge

* Corresponding author at: The Hong Kong Polytechnic University, Room ZS621, South Wing, Block Z, 181 Chatham Road South, Kowloon, Hong Kong, China.
E-mail address: xiaolin.zhu@polyu.edu.hk (X. Zhu).

https://doi.org/10.1016/j.rse.2019.02.019
Received 30 June 2018; Received in revised form 24 January 2019; Accepted 19 February 2019

et al., 2009). Pandey et al. (2017) summarized several algorithms for the relative calibration of DMSP NTL data based on the concept of pseudo-invariant features (PIFs) and found that global-scale calibration methods outperform regionally based calibration methods. The saturation problem resulted from the small (6-bit) quantization and low dynamic range of OLS data, which led to the inability of the OLS to record light brighter than a digital number (DN) value of 63 (Elvidge et al., 1997b). Combined with information about vegetation indices, land surface temperature (LST) or socioeconomic statistics, researchers have developed several methods to effectively mitigate the saturation of OLS data (Lu et al., 2008; Zhang et al., 2013; Zhuo et al., 2015; Hao et al., 2015; Cao et al., 2014). The blooming effect, or overglow, refers to the lighted areas detected by the OLS larger than the geographic extents of the light sources, which leads to the overestimation of the extent of urban areas (Small and Elvidge, 2013). The blooming effect is more serious for coarser nighttime light images (Kyba et al., 2014). For example, the blooming effect was also observed in monthly VIIRS composite data (Levin, 2017) but was not as serious as in DMSP-OLS data. The blooming effect brings difficulties, bias, and challenges to the applications of nighttime light data. However, only a few studies have quantitatively evaluated the blooming effect (Small et al., 2005; Townsend and Bruce, 2010; Hao et al., 2015), and no consensus on blooming effect correction has yet been reached (Bennett and Smith, 2017).

The possible reasons for the blooming effect include the large footprints of the OLS sensor (Elvidge et al., 2004; Elvidge et al., 2013), the scattering of light in the atmosphere, and the accumulation of geolocation errors in the compositing process (Richter, 1996; Small et al., 2005; Small and Elvidge, 2013; Kyba et al., 2014). Existing studies have also found that the blooming effect is related to the equivalent diameter for contiguous lighted areas (Small et al., 2005), light source strength (Townsend and Bruce, 2010), adjacent water or snow surfaces (Bennett and Smith, 2017), and thin clouds (Letu et al., 2015). To reduce the blooming effect in urban area detection, Zhou et al. (2014) used a water mask to exclude pixels with water percentages over 50% along shorelines. Some saturation correction methods, such as the Vegetation Adjusted NTL Urban Index (VANUI) (Zhang et al., 2013) and the Vegetation Temperature Light Index (VTLI) (Hao et al., 2015), can also alleviate the blooming effect. However, since their main purposes are limited, their effectiveness and flexibility to tackle the blooming effect with inadequate validations is not clear. Small et al. (2005) suggested employing a scale-dependent blooming correction procedure after finding a linear relationship between lit area and blooming distance for 10 illuminated islands as samples. However, the method's effectiveness over non-coastal areas has not yet been verified. Townsend and Bruce (2010) developed the Overglow Removal Model (ORM), which corrects the blooming effect by using the relationship between regional light intensity and blooming distance considering the effects of annual atmospheric conditions, topography and elevation. However, the method needs auxiliary data, which may not always be available for locations in developing countries where NTL imagery may provide the most insight regarding economic development. Li et al. (2017) simulated the DMSP-OLS composites from the NPP-VIIRS images by using a power function and a Gaussian low-pass filter. This method can reduce the blooming effect in the simulated DMSP-OLS images because the NPP-VIIRS images have little blooming effect (Bennett and Smith, 2017). However, this method is not able to correct the DMSP-OLS images before 2012, when NPP-VIIRS images became available. Recently, Abrahams et al. (2018) deblurred the DMSP images based on the assumption that light was blurred via a symmetric Gaussian point-spread function (PSF); the dimension of the PSF could be calibrated by the frequency of illumination. This new deblurring method is effective in improving DMSP annual composite images. However, it is limited in processing annual composite images because it needs an auxiliary dataset that records the frequencies of illumination of each pixel, which may be less accurate in cloudy regions such as tropical countries.

To this end, we developed the self-adjusting model (SEAM) based on a spatial response function (SRF) to correct the blooming effect without using other ancillary data. We tested the SEAM model to correct the blooming effect in China and evaluated the effectiveness of the SEAM model in twelve cities with various population scales by comparison with NPP-VIIRS data, the VANUI and VTLI methods, as well as the accuracy of urban area extraction. This simple blooming effect correction model is expected to be used as a preprocessing method for the DMSP-OLS NTL data.

2. Data and methods

2.1. Study area and data

We used DMSP-OLS stable NTL data for China in 2013 (Fig. 1a) to test the blooming correction method proposed by this study. Twelve cities with different size of population and levels of economic development were selected to visually and quantitatively evaluate the performance of the blooming effect correction model. These cities are categorized into six groups by population: > 10 million (Shanghai and Beijing), 5–10 million (Chongqing and Guangzhou), 3–5 million (Harbin and Hangzhou), 1–3 million (Lanzhou and Luoyang), 0.5–1 million (Xinyu and Xingtai), and < 0.5 million (Lhasa and Lijiang). The twelve center cities are marked by black points in Fig. 1(a). Fig. 1(b) shows an enlarged sub-region of the DMSP-OLS image covering Beijing. Because ground truth values of light intensity are not available, the NPP-VIIRS nighttime light images in 2013 are used as a reference to evaluate the effectiveness of the proposed model, assuming the blooming effects in the NPP-VIIRS images are sufficiently weak (Li and Zhou, 2017) (Fig. 1c). The DMSP-OLS and NPP-VIIRS nighttime light data (hereafter DMSP and VIIRS for short) were downloaded from the National Oceanic and Atmospheric Administration (NOAA) National Centers for Environmental Information (http://ngdc.noaa.gov/eog/download.html). The DMSP image downloaded was "F182013.v4c_web.stable_lights.avg_vis.tif". By geolocation processing, the stable lights were summarized to grids with a nominal resolution of 30 arc sec, which equals 1 km at the equator. For convenience, this study used "pixel" to represent the "grid" of the DMSP stable NTL data. Four seasonal VIIRS datasets were downloaded in 2013, and we used the average of the four seasonal VIIRS images as the yearly VIIRS image in 2013 to match the DMSP image. All images were re-projected to the same coordinate system, WGS_1984_UTM49N. Then, the VIIRS data were resampled to the resolution of DMSP images and co-registered to the DMSP images using 20 GCPs selected from isolated cities without saturated pixels (see details in Supplementary Data).

To assess the performance of the proposed blooming effect removal model, we used Moderate Resolution Imaging Spectroradiometer (MODIS) Normalized Difference Vegetation Index (NDVI) and Land Surface Temperature (LST) products to implement two existing DMSP correction models: VANUI (Zhang et al., 2013) and VTLI (Hao et al., 2015). The MODIS monthly composite of NDVI and nighttime LST data for 2013 were selected for this study. The results from the proposed method were compared with these two existing methods. We also compared urban extent extracted from the blooming-adjusted results with a reference urban extent map, the Global Urban Footprint (GUF) map (Esch et al., 2017). The GUF data are provided by the German Aerospace Center (DLR, https://www.dlr.de/) with a spatial resolution of 2.8 arc sec (approximately 75 m in mid-latitudes). This dataset was generated using data collected by the TerraSAR-X/TanDEM-X satellites between 2011 and 2012, which matches the time of the NTL data in this study.

The other data used to aid this research included the ground-level PM2.5 data in 2013 (van Donkelaar et al., 2016) (http://fizz.phys.dal.ca/~atmos/martin/). This dataset is satellite-derived and adjusted by geographically weighted regression with a 0.01° grid. We also used the GlobeLand30-2010 product (Chen et al., 2015; Chen et al., 2016)

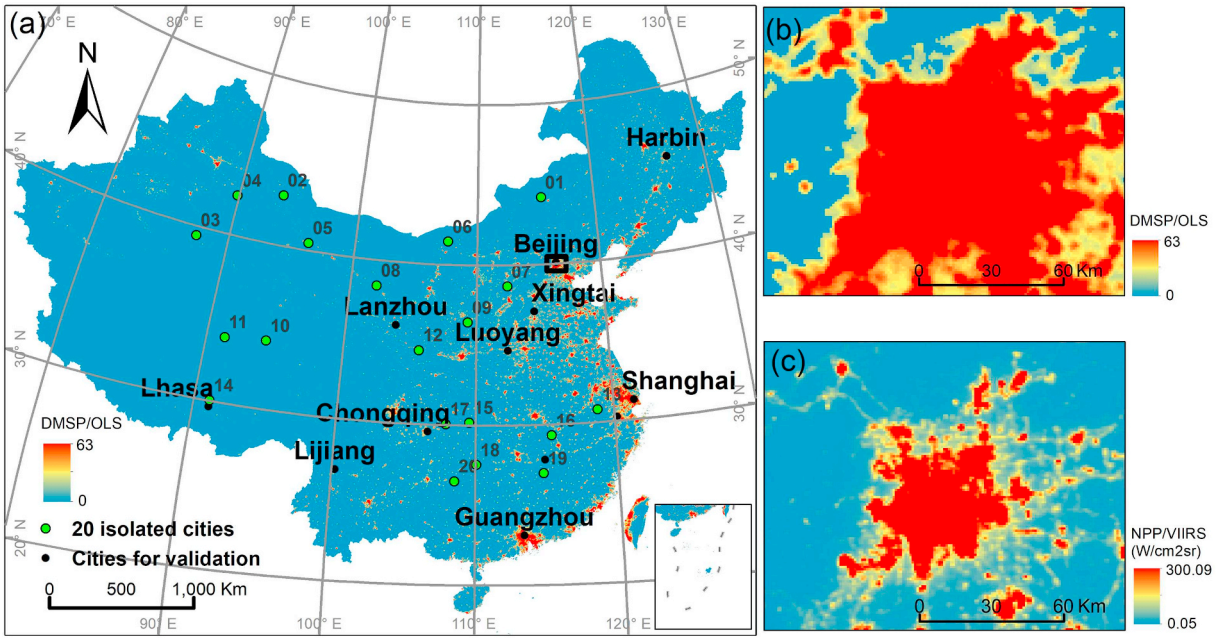

Fig. 1. The DMSP-OLS image of China in 2013 (a). Right column shows the enlarged DMSP-OLS image (b) and NPP-VIIRS image (c) for Beijing (black box in a). The green points with serial numbers are the 20 cities selected to investigate the effective blooming distance (see Table 3). The black points indicate the 12 cities used for evaluation. (For interpretation of the references to color in this figure legend, the reader is referred to the web version of this article.)

(http://www.globeland30.org) to provide further land cover information such as water and urban area.

2.2. Self-adjusting blooming effect correction model

(1) *Theoretical basis*

Theoretically, the blooming effects on individual pixels in DMSP images can be described by the sensor spatial response function (SRF), which is usually modeled as kernel functions, such as the Gaussian function and inverse distance function (Liang, 2003). In this study, the inverse distance function is used to approximate the SRF considering that light intensity attenuates with squared distance:

$$SRF = f(d) = \frac{a}{d^2} \tag{1}$$

where d is the spatial distance corresponding to the sensor ground instantaneous field of view (IFOV) and a is a coefficient. In a satellite image, the SRF implies the degree of signals beyond the pixel size that contribute to the pixel value, i.e., a target pixel value contains the contributions of it neighboring pixels. Therefore, the observed value of a target pixel (R) can be written as:

$$R = \beta \times R_0 + \left(\sum_{i=1}^{N} f(d_i) \times R_i + b \right) \tag{2}$$

The first term on the right side of Eq. (2) indicates the light signal from the target pixel, and the second term is the incoming light from neighboring pixels via the SRF. R_0 is the actual light emitted by the target pixel, β is a coefficient representing the percentage of remaining light after deducting out-scattering of R_0, R_i is the pixel value of the i-th neighboring pixel selected from a moving window, N is the total number of neighboring pixels, and b is the background value. The pixel value R_i of the i-th neighboring pixel includes its actual light and the blooming light it received; R_i in Eq. (2) thus allows the model to count both the direct blooming effect (from neighbors to the target) and the indirect blooming effect (from other pixels to neighbors and then to the target). In this study we assumed that out-scattering is linearly related to the intensity of the light source, i.e., β is a constant value. We also assumed that neighboring pixels that are brighter than the target pixel (i.e., $R_i > R$) make a net blooming contribution because the out-scattering of the target pixel can offset the contribution from darker neighboring pixels. Therefore, the key to remove the blooming effect is to model the ambient incoming light, i.e., to estimate the SRF in Eq. (2). For a given DMSP pixel, the R and R_i of its neighbors are known but not R_0. To make Eq. (2) solvable, we need to search some pixels in the DMSP image that have R_0 equal to zero, i.e., these pixels do not have any artificial light source and are only lit by neighbors due to the blooming effect. We defined these pixels as 'pseudo light pixels' (PLPs), for which the DN values (R') entirely come from the neighboring light pixels:

$$R' = \sum_{i=1}^{N} f(d_i) \times R_i + b \tag{3}$$

Taking Eq. (1) into Eq. (3), we obtain:

$$R' = a \times \sum_{i=1}^{N} \frac{R_i}{d_i^2} + b \tag{4}$$

In Eq. (4), the unknown coefficients a and b can be estimated by regression analysis using the PLPs and their neighboring light pixels.

(2) *Self-adjusting model implementation steps*

Step 1: Search for pseudo light pixels

Based on the above concept, this first step is to find the PLPs in a DMSP image to estimate the coefficients a and b. As the diagram shows in Fig. 2, the intensity of artificial lights in DMSP images generally decreases from a city center to its edges (Zhou et al., 2015), with the brightest pixels (e.g., DN = 63) located in the city centers and the darkest pixels (DN = 0) close to rural areas (background areas). We thus assume that PLPs can be selected from pixels next to the urban edges, i.e., the pixel itself shows weak brightness (pixel value > 0) but one or more of its eight neighbors are dark (pixel value = 0) in the DMSP/OLS images (e.g., the light gray pixels in Fig. 2). As a result, the DN values of these pixels should mainly come from their neighboring

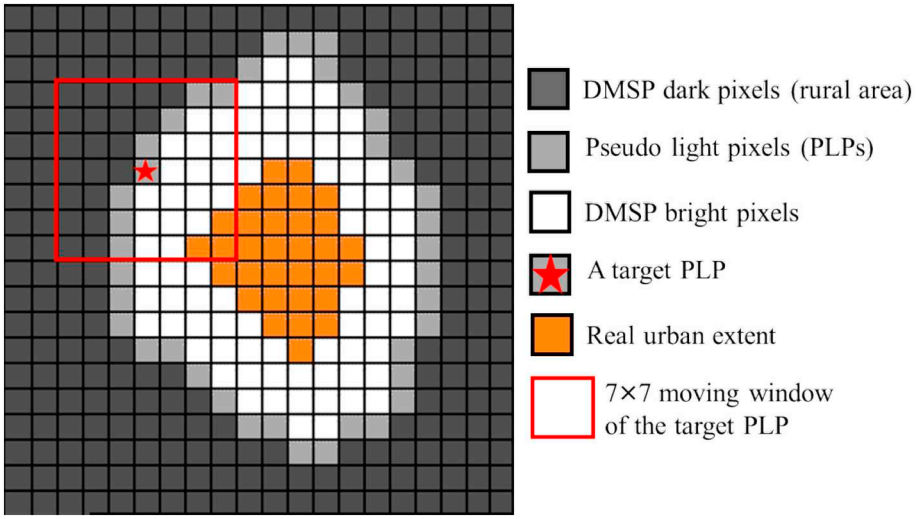

Fig. 2. Diagram of selecting pseudo light pixels (PLPs) and their effective neighboring pixels within a 7 × 7 moving window.

pixels due to the blooming effect. These pixels are selected as the PLPs and their pixel values can be described by Eq. (4).

Step 2: Select effective neighboring pixels for PLPs

For each PLP, we need to select its effective neighboring pixels, i.e., the pixels within the effective blooming distance, for calculating its value by Eq. (4). By visual comparison between DMSP image and a referenced urban extent derived from a global 30-m land cover map (Chen et al., 2015) for 20 isolated cities in China with relatively regular shape (Fig. 1a, marked by green points and labeled by numbers), the urban extent from GlobeLand30 was used as a reference to measure the blooming effect distance of DMSP data. For each PLP of a city, we can search a nearest distance to the urban region of GlobeLand30, and the average distance of all the PLPs to their nearest urban region represent the effective blooming distance of the city. The effective blooming distance ranges from 2.22 to 4.38 km (see Table 3 in Discussion Session for details), and the average value is 3.53 km, which is equivalent to 3.5 pixels in DMSP images. Based on Eq. (1), the neighboring pixels beyond 3.5 km should have very weak influence on PLPs. Therefore, a 7 × 7 moving window (with a PLP as the center) was suggested to search the effective neighboring pixels (Fig. 2). For each PLP, only the pixels within the 7 × 7 window with DN values larger than that of the PLP are chosen as effective neighboring pixels to compute the weighted sum in Eq. (4). The spatial distance between the PLP and its neighboring pixels is calculated as the Euclidean distance between the centers of the pixels.

Step 3: Remove blooming effect for each bright DMSP pixel

For each bright DMSP pixel with DN larger than 0 (named as the target pixel), we can apply Eq. (2) to estimate the light intensity excluding the blooming effect if we know the coefficients $\boldsymbol{a}$ and $\boldsymbol{b}$. In one DMSP image, we can select enough PLPs and their effective neighboring pixels following step 1 and 2 and then estimate $\boldsymbol{a}$ and $\boldsymbol{b}$ by linear regression. However, the estimated $\boldsymbol{a}$ and $\boldsymbol{b}$ are global parameters for the entire DMSP image, which may not be optimal values for removing the blooming effect for all individual DMSP pixels. Considering that the intensity of the blooming effect might be affected by some local factors, such as the total light intensity of surrounding urban pixels (Townsend and Bruce, 2010), local atmospheric conditions (Small and Elvidge, 2013) and adjacent water bodies or snow (Bennett and Smith, 2017), the coefficients in Eq. (4) may change pixel-by-pixel, and local PLPs were thus selected to estimate the coefficients for each target pixel. Specifically, for each DMSP pixel with DN larger than 0, PLPs were selected within a radius range of 150 km; a 150-km radius was used because (1) enough PLPs can be selected and (2) atmospheric conditions (e.g., particulate matter concentrations, $PM_{2.5}$ and PM_{10}) within this range are relatively uniform (Hu et al., 2014). For each PLP, its effective neighboring pixels were selected within the 7 × 7 window following step 2. Then, the values of PLPs and the weighted sum of their effective neighboring pixels were used as dependent and independent variables to estimate parameters a and b in Eq. (4) by ordinary least squares linear regression. Finally, for the target DMSP pixel, its pixel value without blooming effects (R^*) can be estimated by:

$$R^* = R - \left(\hat{a} \times \sum_{i=1}^{N} \frac{R_i}{d_i^2} + \hat{b} \right) \quad (5)$$

where R^* is the first term on the right side of Eq. (2), $\beta \times R_0$, the real artificial light after deducting out-scattering. $\hat{a}$ and $\hat{b}$ are estimated coefficients. R_i is the DN value of the effective neighboring pixels of the target pixel and $R_i > R$. Extremely large difference between adjacent pixels may exist in the original DMSP image. This extreme large difference will lead to unreliable results (e.g., negative brightness values) of blooming adjustment using Eq. (5). To mitigate the impact of this extreme situation, we then introduced a mean filter by using a 3 × 3 moving window to reduce the extremely large differences among adjacent pixels while maintaining the spatial pattern of the original DMSP image.

2.3. Performance assessment of blooming effect removal

To evaluate the performance of SEAM for blooming effect removal, we compared SEAM with two other vegetation adjusted methods, VANUI (Eq. 6) and VTLI (Eq. 7), to correct the DMSP data. VANUI combines the MODIS NDVI with the NTL data based on the hypothesis that the vegetation abundance is highly negatively correlated with the distribution of impervious surfaces (Zhang et al., 2013). VTLI incorporates the land surface temperature (LST) information with the vegetation index due to the temperature being higher in the center of the city (Hao et al., 2015). The monthly maximum composite of NDVI and nighttime LST for MODIS in 2013 was used to calculated VANUI and VTLI, respectively:

$$\text{VANUI} = (1-\text{NDVI}) \times \text{NTL} \quad (6)$$

$$\text{VTLI} = (1-\text{NDVI}) \times \text{LST} \times \text{NTL} \quad (7)$$

In summary, for the original DMSP image, three blooming-adjusted

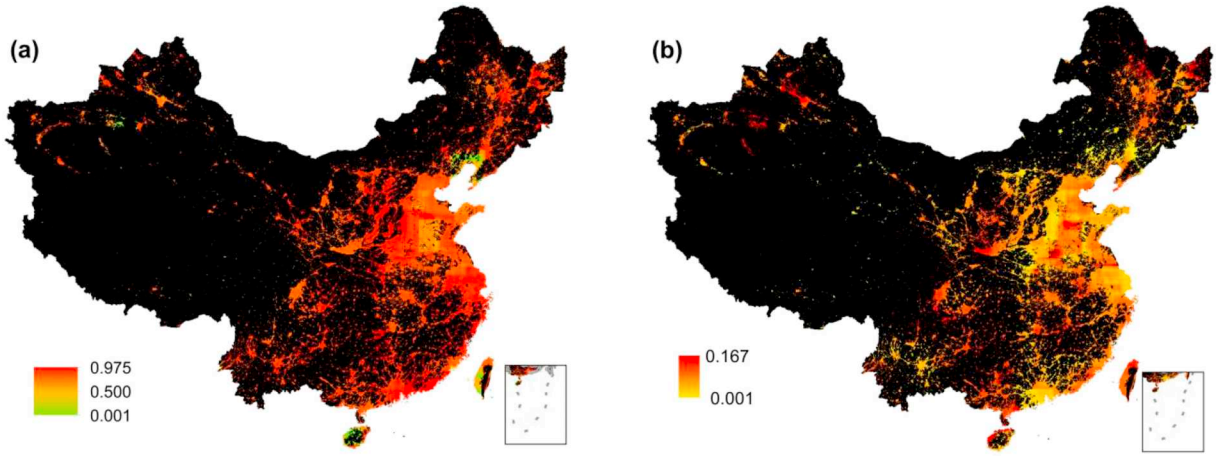

Fig. 3. Regression results for pixel-based regression models; (a) coefficients of determination (R^2), and (b) regression coefficient *a*.

results were obtained by the proposed SEAM model (hereafter DMSP-BC) and the VANUI and VTLI methods, respectively. Two evaluation indicators, the correlation coefficient between the evaluated image and the reference image (i.e., VIIRS image) and the spatial variability of the evaluated image, were used to assess the effectiveness of different models for blooming effect removal.

1) *Correlation coefficients (R) between VIIRS images and the evaluated images.*

R is used to measure the correlation between VIIRS image and DMSP, DMSP-BC, VANUI and VTLI images. The SEAM model cannot remove the saturation effect, and pixels with DN values of 63 in the DMSP images and corresponding areas in the VIIRS images were thus excluded when calculating the correlation coefficients. If blooming effect correction is effective, the blooming-adjusted images are expected to have higher *R* values with the VIIRS image than with the original DMSP image. The correlation coefficients were computed for each city using pixels within the minimum bounding rectangle of the city extent detected from the VIIRS image.

2) *Spatial variability of pixel values within urban areas of each nighttime image.*

Theoretically, the blooming effect makes DMSP images 'smooth' and decreases the spatial variability of pixel values in urban regions compared with the corresponding VIIRS images, which have minimal blooming effects. After correcting the blooming effect with the SEAM method, the spatial variability of DMSP-BC is expected to be higher than that of the original DMSP image. Since the DN values of DMSP images and VIIRS images are not comparable in value, we used the coefficient of variation (CV) to measure the relative spatial variability:

$$CV = std(R)/mean(R) \quad (8)$$

where *R* is the DN value in each city and *std*(*R*) and *mean*(*R*) are the standard deviation and mean of the DN values, respectively. *CV* was calculated for VIIRS, DMSP, DMSP-BC, VANUI and VTLI images.

We also evaluated the performance of NTL data for urban area extraction by comparing the results from DMSP and DMSP-BC with Global Urban Footprint (GUF) data as reference data. Because GUF data have higher spatial resolution (approximately 75 m in mid-latitudes), we first aggregated the data to 1-km spatial resolution (GUF-1 km) to match the DMSP data. Then, we adopted the local optimized threshold method (Cao et al., 2009) to extract urban areas from DMSP and DMSP-BC images. The local optimized threshold is the one among all tested thresholds that can obtain the highest Kappa coefficient of the extracted urban areas using GUF-1 km as reference data.

3. Results

3.1. Parameter estimation in the SEAM model

As explained in Section 2.2, for each pixel with DN values lager than 0 in the DMSP image of China, a local regression model was built to estimate parameters *a* and *b* using PLPs selected in a neighborhood. Fig. 3 shows the spatial distribution of the pixel-based regression results. The coefficients of determination (R^2) for the pixel-based regression models are plotted in Fig. 3(a). Over 97% of the pixels achieve a high coefficient of determination (> 0.7), whereas some pixels in coastal areas and inland northwest areas have lower coefficients of determination. The regression models for pixels with coefficients of determination < 0.7 were replaced by those with the highest coefficients of determination close to these pixels. Fig. 3(b) indicates the spatial distribution of regression coefficient *a* in Eq. (4), which represents the intensity of the blooming effect. A higher regression coefficient *a* indicates a stronger blooming effect and more lights scattered from a pixel to its neighborhood. We found that the regression coefficient *a* is positively correlated with annual mean $PM_{2.5}$ concentrations ($R = 0.5677$, $p < 0.0001$) for all of China, excluding the pixels with $DN = 0$. This result suggests that the intensity of the blooming effect may be influenced by atmospheric conditions.

3.2. Visual evaluation

Fig. 4 shows the original DMSP images, the VIIRS images, the DMSP-BC images, and the VANUI and VTLI images of the twelve cities with populations from < 0.5 million to over 10 million. To make these images visually comparable, the NPP-VIIRS, VANUI and VTLI images were linearly stretched to the range of the DMSP data using the minimum and maximum pixel values. It can be observed from Fig. 4 that the DMSP data suffered from a strong blooming effect when compared with the VIIRS images, whereas the DMSP-BC images could shrink the boundaries of urban areas and decrease the values for urban outskirts. Compared with the DMSP images, the DMSP-BC, VANUI and VTLI images have higher spatial similarity with the VIIRS images. In large cities, such as Shanghai, Beijing, Guangzhou and Hangzhou, we can observe some line objects (e.g., roads) in the DMSP-BC or VIIRS images that are totally covered by the blooming effect in the original DMSP images. However, for Shanghai and Beijing in the VANUI and VTLI images, the urban centers have low DN values, which might result from the high vegetation coverage in these regions. In Chongqing, Harbin, Lanzhou, Luoyang, Xinyu, Xingtai, Lhasa and Lijiang, dark pixels in the VIIRS images (the rural areas) were brightened in the original DMSP images due to the effect of blooming, whereas these pixels are adjusted to nearly zero in the DMSP-BC images. Visual

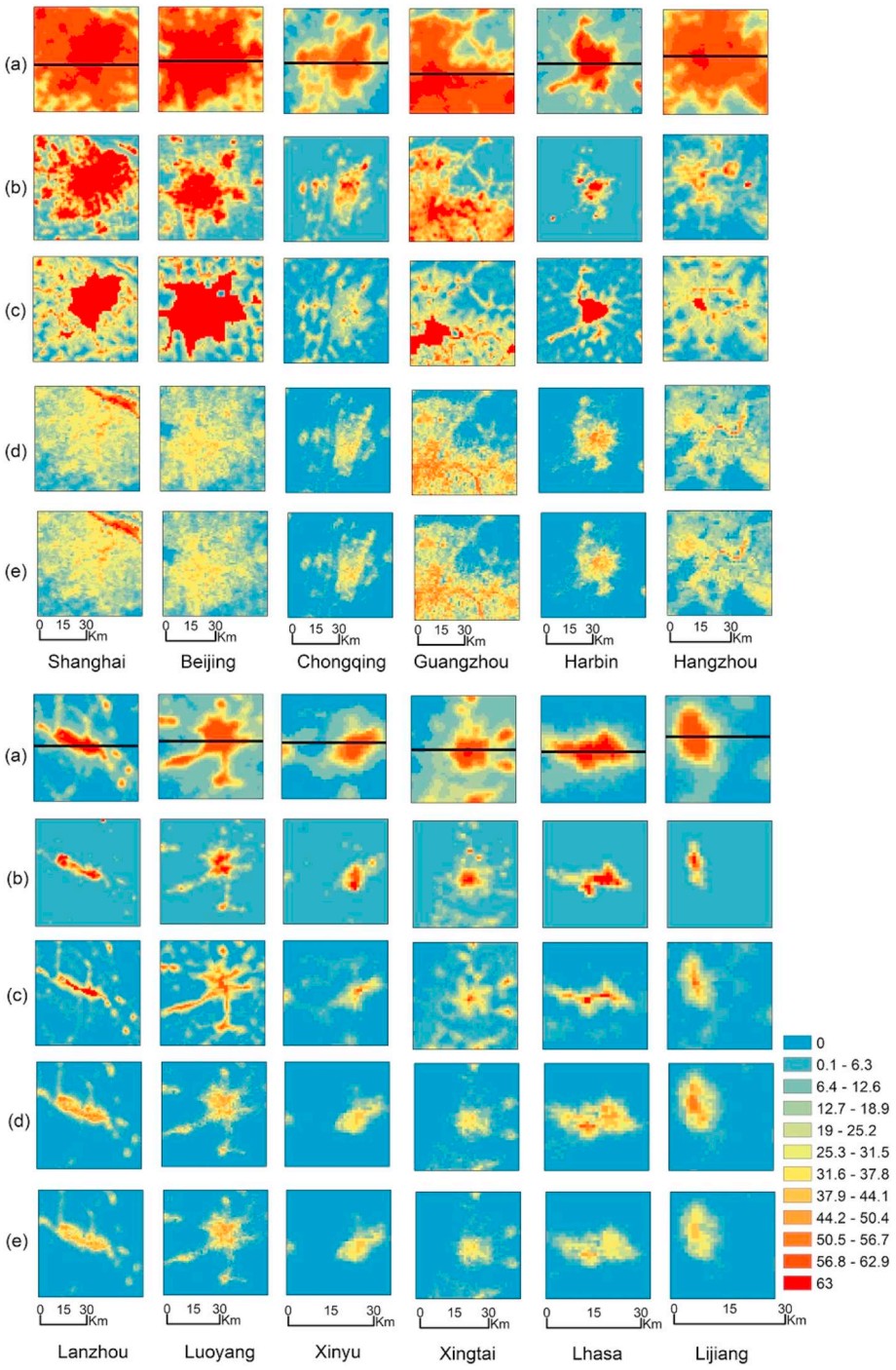

Fig. 4. Comparison of the NTL images in the twelve cities of China: (a) the original DMSP-OLS images, (b) the NPP-VIIRS images, (c) the DMSP-BC images, (d) the VANUI images, and (e) the VTLI images. The black lines are transects whose values are plotted in Fig. 5.

inspection of these twelve cities indicates that the SEAM model can mitigate the blooming effect of the original DMSP image.

Fig. 5 shows the DN values of the transects in the DMSP images (blue lines), VIIRS images (black lines) and DMSP-BC images (red lines) for the twelve cities. It can be observed that all three NTL images have lower DN values in rural areas and higher values in urban areas, especially in the city center. The values of the DMSP-BC images are smaller than those of the original DMSP images after removing the blooming parts, especially in the rural regions. These transects also show that the variations of DN values in the DMSP-BC images have greater similarity with the VIIRS images compared with the DMSP images. Moreover, the variation of DN values in the urban areas of the DMSP images is smaller than those of the DMSP-BC and VIIRS images. For transects of Shanghai, Beijing and Guangzhou (Fig. 5a, b and d), many saturated values in the DMSP images close to urban cores were also adjusted into lower values in the DMSP-BC images. This result suggests that the SEAM model can also partly remove the effect of saturation. In the rural areas where DN values of VIIRS are close to zero, the DMSP images maintain high values of approximately 10–20 (e.g., the west part of Lanzhou, Luoyang and Xinyu in Fig. 5g, h and i) due to the blooming effect, and the DN values of these pixels in the DMSP-BC image were adjusted to 0–5. These transects suggest that the SEAM model can effectively remove the blooming effect and partly remove the saturation effect in DMSP images.

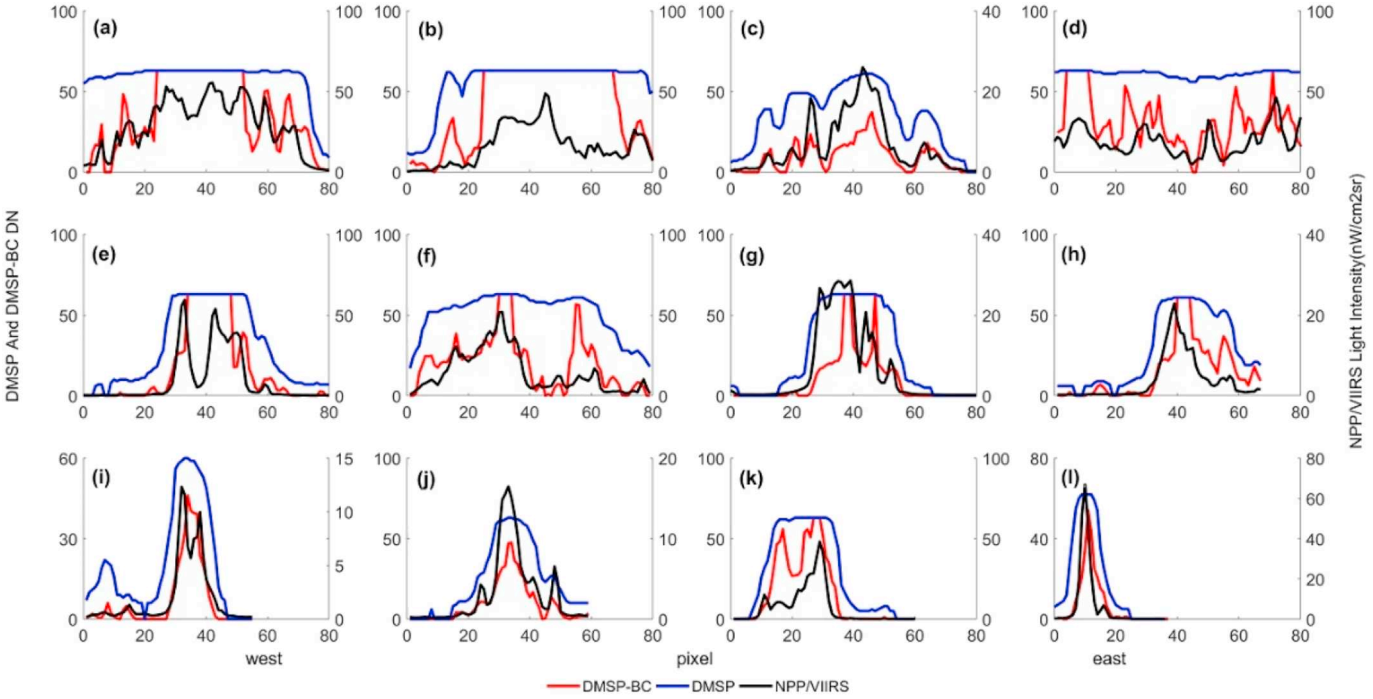

Fig. 5. Profiles of transects (the black lines in Fig. 4) of Shanghai (a), Beijing (b), Chongqing (c), Guangzhou (d), Harbin (e), Hangzhou (f), Lanzhou (g), Luoyang (h), Xinyu (i), Xingtai (j), Lhasa (k), and Lijiang (l) from the DMSP, VIIRS and DMSP-BC images.

3.3. Quantitative evaluation

Table 1 lists the correlation coefficients (R) with VIIRS images for DMSP, DMSP-BC, VANUI and VTLI and CV values calculated by Eq. (8) for DMSP, VIIRS, DMSP-BC, VANUI and VTLI in twelve selected cities and the whole of China, excluding pixels with DN equal to 0 in the DMSP-BC image. When comparing original DMSP and DMSP-BC images, the correlation coefficients with VIIRS images in the whole of China are 0.62 and 0.69 for the original DMSP and DMSP-BC images, respectively, whereas all twelve cities have higher correlation coefficients after blooming effect correction by the SEAM model. The increase of the correlation coefficients indicates that the DMSP-BC images are more similar to the VIIRS images compared with the original DMSP images. In terms of spatial variability, the images after blooming effect removal for all twelve cities can have higher CVs than the original DMSP images. The CV values of the twelve cities from DMSP-BC are between the CV values from the DMSP and VIIRS images, and the CVs of the whole of China are 1.53, 0.94 and 2.64 for DMSP-BC, DMSP, and VIIRS images, respectively, which suggests that the spatial variability of the DMSP images was enhanced after blooming effect correction. However, the spatial variability of the DMSP-BC images is still not as high as that of the VIIRS images. The possible reasons include the existence of saturated pixels, the discrepancy of spatial resolutions between DMSP and VIIRS, and the remaining blooming effect.

The results in Table 1 show that in some cities the DMSP-BC images from SEAM perform better than VANUI and VTLI. The correlation results show lower values for VANUI and VTLI in Shanghai, Beijing, Guangzhou, Hangzhou, Lhasa and Lijiang. The possible reason for this result may be that the high percentage of green space makes the assumption of the two indexes invalid. For the other cities, SEAM's results are comparable with those of VANUI and VTLI. These results suggest that the auxiliary data, such as NDVI and LST, may introduce extra errors in blooming correction. The CV values indicate similar spatial variabilities for SEAM, VANUI and VTLI. We noticed that VANUI and

Table 1
The quantitative evaluation of the DMSP, DMSP-BC, VANUI and VTLI images for the twelve cities and all of China.

City/province	Population[a] (million)	Correlation with VIIRS (R)				Spatial variability (CV)				
		DMSP	DMSP-BC	VANUI	VTLI	DMSP	VIIRS	DMSP-BC	VANUI	VTLI
Shanghai/Shanghai	13.64	0.643	0.769	0.648	0.661	0.409	1.080	0.797	0.535	0.523
Beijing/Beijing	12.45	0.629	0.784	0.751	0.760	0.533	1.594	1.103	0.932	0.948
Chongqing/Chongqing	8.52	0.785	0.801	0.841	0.845	0.676	1.090	1.021	1.376	1.394
Guangzhou/Guangdong	6.87	0.687	0.746	0.694	0.691	0.690	1.601	1.075	1.098	1.139
Harbin/Heilongjiang	4.74	0.612	0.768	0.775	0.781	0.917	3.128	1.721	2.084	2.111
Hangzhou/Zhejiang	4.51	0.636	0.698	0.605	0.615	0.332	1.070	0.705	0.720	0.724
Lanzhou/Gansu	2.47	0.702	0.747	0.772	0.780	0.951	2.453	1.590	1.214	1.246
Luoyang/Henan	1.93	0.771	0.797	0.877	0.882	0.786	1.652	1.311	1.327	1.352
Xinyu/Jiangxi	0.89	0.731	0.744	0.820	0.824	0.787	1.681	1.305	1.376	1.392
Xingtai/Hebei	0.87	0.725	0.738	0.811	0.815	0.717	1.527	1.205	1.176	1.193
Lhasa/Xizang	0.30	0.680	0.685	0.649	0.662	0.796	1.904	1.314	1.098	1.122
Lijiang/Yunnan	0.15	0.706	0.877	0.808	0.770	0.920	2.287	1.470	1.228	1.184
Whole China	/	0.619	0.694	0.702	0.711	0.936	2.639	1.530	1.538	1.574

[a] The populations of each city in 2013 were collected from the China City Statistical Yearbook 2014 (National Bureau of Statistics of China, 2014).

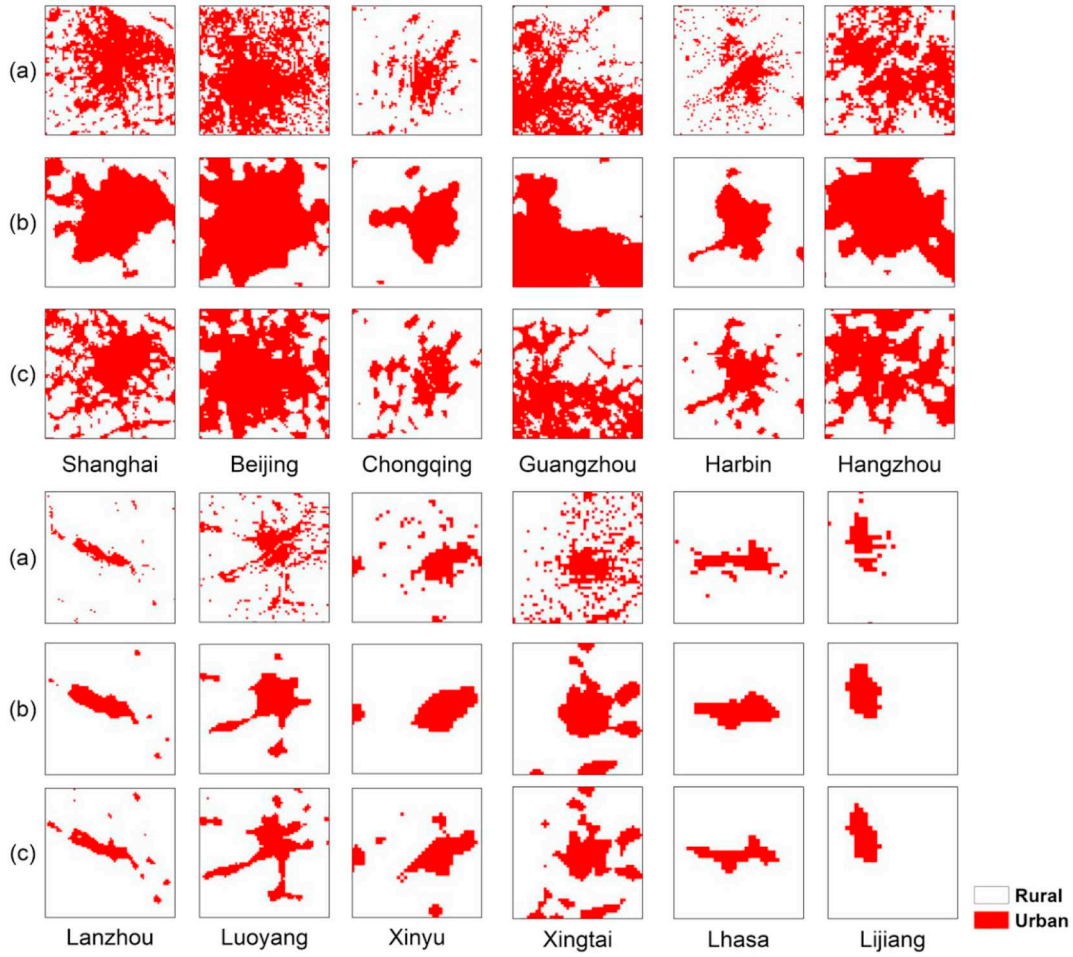

Fig. 6. Comparison of the urban area of (a) the Global Urban Footprint images at 1-km resolution (GUF-1 km) and urban area extracted from (b) DMSP-OLS images and (c) DMSP-BC images in the twelve cities of China.

VTLI show comparable or even better results than SEAM in some cities; however, the axillary datasets required by these methods impede their applicability.

3.4. Urban area extraction

The results of urban areas extraction are shown in Fig. 6 and Table 2. Fig. 6 indicates that the spatial distributions of the urban areas are more similar to the GUF data after blooming effect removal. For example, the urban region of Shanghai extracted from the DMSP data by the local optimal threshold is only the urban core area, whereas the DMSP-BC result could extract the tiny urban regions that also exist in the GUF image. Table 2 lists the urban areas of the 12 cities extracted from the DMSP and DMSP-BC images as well as the reference urban areas from the GUF data. Table 2 also shows differences in urban areas between GUF and DMSP (denoted as Difference_DMSP) and between GUF and DMSP-BC (denoted as Difference_DMSP-BC). From Table 2 we find that the areas of the urban areas extracted from the DMSP-BC images are closer to the reference values than those from the DMSP data. The kappa coefficients in Table 2 also confirm that urban areas extracted from DMSP-BC are more similar to the GUF reference than those from DMSP. In conclusion, DMSP images after removing the blooming effect by the SEAM model can obtain more accurate urban extents than the original DMSP data.

Table 2
Urban areas extracted from the DMSP and DMSP-BC images for the twelve cities (unit = km^2).

City/province	Kappa for DMSP	Kappa for DMSP-BC	Area from DMSP	Area from DMSP-BC	Area from GUF	Difference_DMSP	Difference_DMSP-BC
Shanghai/Shanghai	0.7302	0.7382	2399	2798	2798	399	0
Beijing/Beijing	0.7756	0.8437	3754	4294	4359	605	65
Chongqing/Chongqing	0.5181	0.6604	1058	992	711	347	281
Guangzhou/Guangdong	0.7364	0.7950	11,274	10,962	9221	2053	1741
Harbin/Heilongjiang	0.6718	0.8120	975	1153	1266	291	113
Hangzhou/Zhejiang	0.6200	0.6317	2005	1908	1712	293	196
Lanzhou/Gansu	0.5925	0.7823	359	320	330	29	10
Luoyang/Henan	0.6652	0.8639	518	596	672	154	76
Xinyu/Jiangxi	0.6401	0.7305	177	205	209	32	4
Xingtai/Hebei	0.4713	0.6916	500	495	576	76	81
Lhasa/Xizang	0.3767	0.4581	120	86	99	21	13
Lijiang/Yunnan	0.7160	0.8843	65	56	59	6	3

Table 3
Effective blooming distance for 20 cities in China.

Serial number	City/province	Effective blooming distance (km)	Average light intensity of the city (DN)	$PM_{2.5}$ concentration ($\mu g/m^3$)	Water area surrounding the city (km^2)[a]
01	Xilinhot/Inner Mongolia	4.08	15.37	16.77	1.24
02	Hami/Xinjiang	3.31	23.13	18.30	0.21
03	Korla/Xinjiang	2.49	13.93	17.80	0.46
04	Turpan/Xinjiang	2.22	14.70	16.39	0.00
05	Jiuquan/Gansu	2.84	14.14	29.10	0.35
06	Bayannur/Inner Mongolia	2.36	23.10	23.79	0.00
07	Xinzhou/Shanxi	3.27	19.15	31.61	0.00
08	Jinchang/Gansu	4.38	16.60	36.35	1.18
09	Yan'an/Shaanxi	2.73	10.65	38.20	1.42
10	Yushu/Qinghai	3.36	13.38	31.12	1.00
11	Delingha/Qinghai	3.63	13.40	43.73	0.84
12	Tianshui/Gansu	4.39	14.92	6.65	3.89
13	Xuancheng/Anhui	3.31	12.36	64.36	0.22
14	Lhasa/Xizang	4.35	18.54	29.64	9.99
15	Enshi/Hubei	3.07	16.61	27.83	0.18
16	Jiujiang/Jiangxi	3.74	19.66	29.19	3.45
17	Chongqing/Chongqing	4.32	14.29	29.35	0.59
18	Huaihua/Hunan	4.33	17.16	39.42	10.56
19	Ji'an/Jiangxi	4.01	14.72	31.50	0.21
20	Kaili/Guizhou	4.33	15.40	32.26	2.11
	Average	3.53	16.06	29.67	1.89

[a] The water area surrounding each city was calculated by the range of effective blooming distance for each city. Both the urban extent and water surface were provided by the GlobeLand30–2010 land cover product.

4. Discussion and conclusions

DMSP datasets are useful for studying regional economic development because of their strong relationship with economic development, energy consumption and population. However, DMSP datasets severely suffer from saturation and blooming effects. This research proposed a simple blooming effect correction method, the self-adjusting model (SEAM), based on spatial response functions without using any ancillary data. The SEAM model was tested in the whole of China and produced blooming-effect-corrected images, i.e., DMSP-BC, compared with the original DMSP and NPP-VIIRS images. The visual and quantitative evaluations as well as the results of urban area extraction suggested that the SEAM model can largely remove the blooming effect in the original DMSP dataset and enhance its spatial quality.

The greatest strength of the SEAM method is that it estimates the important parameters in the spatial spread function from the DMSP image itself rather than requiring any other ancillary data, and the estimated parameters are then used to remove blooming effects on all DMSP pixels. This advantage makes the SEAM method very applicable and easy to implement. In contrast, existing methods, such as the frequency threshold method (Small et al., 2005) and the overglow removal model (Townsend and Bruce, 2010), need other ancillary datasets and extra effort. The frequency threshold method (Small et al., 2005) needs urban extent derived from Landsat images to determine the optimal frequency threshold, and this study also suggested that it is very difficult to find one threshold that works for a majority of cities in the world. The overglow removal model is an iterative process that needs administrative division boundaries as masks and census population data to stop the iterative process (Townsend and Bruce, 2010); moreover, this model was only tested in Australia due to the availability of an ancillary dataset.

The second strength of the SEAM method is that the SEAM model was developed based on reasonable assumptions, one of which is that DMSP images have pseudo light pixels (PLPs), i.e., pixels containing little artificial light source but lit by neighboring light sources. The pixels adjacent to the background were defined as PLPs, and their neighbors with larger DN values were used as neighboring light sources. Such PLPs should exist in any countries that have cities visible in the DMSP images. Another assumption is that the effective blooming distance is approximately 3.5 km, and a 7 × 7 moving window was thus used to removing blooming from the neighboring pixels. We investigated the effective blooming distance in 20 isolated cities using a land cover product, GlobeLand30 (Chen et al., 2015; Chen et al., 2016). Table 3 lists the effective blooming distances and the average light intensities measured from the DMSP image, mean concentrations of $PM_{2.5}$ at ground-level (van Donkelaar et al., 2016) and neighboring water areas of the 20 cities. The results indicate that the smallest distance is 2.22 km in Turpan (No. 04 in Fig. 1a) and the largest is 4.38 km in Jinchang (No. 08 in Fig. 1a). The average distance for 20 cities is 3.53 km, which is equivalent to 3.5 pixels in DMSP images. Therefore, it is reasonable to use the 7 × 7 window to define the neighboring pixels whose blooming light can reach the pixel at the window center. We also found that this effective blooming distance is not related to the average light intensity of the city ($R = 0$, $p = 0.50$) and $PM_{2.5}$ concentration ($R = 0.10$, $p = 0.35$), which suggests that the 7 × 7 window is good for cities with different sizes and under different atmospheric conditions. An experiment using different window sizes suggests that the proposed method is not very sensitive to the window size (see Supplementary Data). Therefore, the 7 × 7 window should obtain acceptable accuracy and is recommended for most areas, although we suggest further studies to test the parameter in more countries. Note that the effective blooming distance may be longer than 3.5 km in coastal cities or cities with many water surfaces. From the 20 cities listed in Table 3, the effective blooming distance is positively correlated to the water area surrounding a city ($R = 0.53$, $p < 0.05$). Although the 7 × 7 window can obtain satisfactory results of blooming effect removal by the SEAM model for coastal cities (see Supplementary Data), a larger window is recommended for processing DMSP images in coastal areas.

The third strength is that the proposed SEAM method optimizes the parameters in the adjustment model locally rather than globally. Blooming effect intensity, represented by the regression coefficient a (Fig. 3b), was found to be positively correlated with the annual mean $PM_{2.5}$ concentration ($R = 0.5677$, $p < 0.0001$), which suggests that the blooming effect is strengthened by the scattering of aerosol particles in the air (Xu et al., 2015). Considering that the $PM_{2.5}$ concentration varies in space, it is necessary to build the adjusting model for removing the blooming effect in DMSP images locally.

In this study, we only tested the SEAM model in China, and more countries should be used to further evaluate the effectiveness of our method. We did not compare the SEAM model with many other

methods, such as the ORM model (Townsend and Bruce, 2010) because it is difficult to collect the auxiliary data required by these methods. Some saturation pixels remained in the blooming-effect-corrected images for big cities, e.g., Shanghai, Beijing, Guangzhou and Harbin (Fig. 4). Saturation correction methods (Zhang et al., 2013; Zhuo et al., 2015; Hao et al., 2015) could further improve the quality of DMSP data after applying the proposed method. By mitigating the blooming effect in DMSP images by the proposed SEAM method, the corrected DMSP images are expected to map the socioeconomic parameters and monitor urbanization processes with improved performance (see an example in the Supplementary Data). Note that blooming correction is not necessary for other applications such as mapping light pollution. Due to its simple principle, the SEAM method has the potential to produce blooming-adjusted DMSP NTL images in large areas. The SEAM model requires computational resources to select PLPs and build regression models for each pixel. Processing the entire region of China (5074 × 4001 pixels) required approximately 17 h using one CPU of a quad-core desktop computer (3.3 GHz, Intel(R) Core(TM) i5-4590). The computational efficiency can be further improved by parallel computing and high-performance computers.

Acknowledgements

This study was supported by the Taishan Scholar Program of Shandong Province, China, the Research Grants Council of Hong Kong (No. 25222717), the National Natural Science Foundation of China (Nos. 41701627 and 41701378), the Fund for Creative Research Groups of the National Natural Science Foundation of China (41621061), and a research grant from The Hong Kong Polytechnic University (No. 1-ZE6Q).

Appendix A. Supplementary data

Supplementary data to this article can be found online at https://doi.org/10.1016/j.rse.2019.02.019.

References

Abrahams, A., Oram, C., Lozano-Gracia, N., 2018. Deblurring DMSP nighttime lights: a new method using Gaussian filters and frequencies of illumination[J]. Remote Sens. Environ. 210, 242–258.
Bennett, M.M., Smith, L.C., 2017. Advances in using multitemporal night-time lights satellite imagery to detect, estimate, and monitor socioeconomic dynamics. Remote Sens. Environ. 192, 176–197.
Butt, M.J., 2012. Estimation of light pollution using satellite remote sensing and geographic information system techniques. GISci. Remote Sens. 49, 609–621.
Cao, X., Chen, J., Imura, H., Higashi, O., 2009. A SVM-based method to extract urban areas from DMSP-OLS and SPOT VGT data. Remote Sens. Environ. 113, 2205–2209.
Cao, X., Wang, J., Chen, J., Shi, F., 2014. Spatialization of electricity consumption of China using saturation-corrected DMSP-OLS data. Int. J. Appl. Earth Obs. Geoinf. 28, 193–200.
Chen, J., Chen, J., Liao, A., Cao, X., Chen, L., Chen, X., He, C., Han, G., Peng, S., Lu, M., Zhang, W., Tong, X., Mills, J., 2015. Global land cover mapping at 30 m resolution: a POK-based operational approach. ISPRS-J. Photogramm. Remote Sens. 103, 7–27.
Chen, X., Cao, X., Liao, A., Chen, L., Peng, S., Lu, M., Chen, J., Zhang, W., Zhang, H., Han, G., Wu, H., Li, R., 2016. Global mapping of artificial surfaces at 30-m resolution. Sci. China-Earth Sci. 59 (12), 2295–2306. https://doi.org/10.1007/s11430-016-5291-y.
Cinzano, P., Falchi, F., Elvidge, C.D., 2001. The first world atlas of the artificial night sky brightness. Mon. Not. Roy. Astron. Soc. 328 (3), 689–707.
Elvidge, C.D., Baugh, K.E., Kihn, E.A., Kroehl, H.W., Davis, E.R., Davis, C.W., 1997a. Relation between satellite observed visible-near infrared emissions, population, economic activity and electric power consumption. Int. J. Remote Sens. 18 (6), 1373–1379.
Elvidge, C.D., Baugh, K.E., Kihn, E.A., Kroehl, H.W., Davis, E.R., 1997b. Mapping city lights with nighttime data from the DMSP operational linescan system. Photogramm. Eng. Remote. Sens. 63, 727–734.
Elvidge, C.D., Imhoff, M.L., Baugh, K.E., Hobson, V.R., Nelson, I., Safran, J., Tuttle, B.T., 2001. Night-time lights of the world: 1994–1995. ISPRS-J. Photogramm. Remote Sens. 56 (2), 81–99.
Elvidge, C.D., Safran, Jeffrey, Nelson, I., Tuttle, B., Hobson, V. Ruth, Baugh, Kimberly E., Dietz, John B., Erwin, Edward H., Lunetta, R., Lyon, J., 2004. Area and Positional Accuracy of DMSP Nighttime Lights Data. CRC Press, Boca Raton, FL, USA.
Elvidge, C.D., Cinzano, P., Pettit, D.R., Arvesen, J., Sutton, P., Small, C., Nemani, R., Longcore, T., Rich, C., Safran, J., Weeks, J., Ebener, S., 2007. The Nightsat mission concept. Int. J. Remote Sens. 28 (12), 2645–2670.
Elvidge, C.D., Ziskin, D., Baugh, K.E., Tuttle, B.T., Ghosh, T., Pack, D.W., Erwin, E.H., Zhizhin, M., 2009. A fifteen year record of global natural gas flaring derived from satellite data. Energies 2, 595–622.
Elvidge, C.D., Baugh, K., Zhizhin, M., Hsu, F.-C., 2013. Why VIIRS data are superior to DMSP for mapping nighttime lights? In: Proceedings of the 35th Meeting of the Asia Pacific Advanced Network 2013. vol. 35. pp. 62–69.
Elvidge, C.D., Baugh, K.E., Zhizhin, M., Hsu, F.-C., Ghosh, T., 2017. VIIRS night-time lights. Int. J. Remote Sens. 38 (21), 5860–5879.
Esch, T., Heldens, W., Hirner, A., Keil, M., Marconcini, M., Roth, A., Zeidler, J., Dech, S., Strano, E., 2017. Breaking new ground in mapping human settlements from space-The Global Urban Footprint. ISPRS-J. Photogramm. Remote Sens. 134, 30–42.
Falchi, F., Cinzano, P., Duriscoe, D., Kyba, C.C.M., Elvidge, C.D., Baugh, K., Portnov, B.A., Rybnikova, N.A., Furgoni, R., 2016. The new world atlas of artificial night sky brightness. Sci. Adv. 2 (6), e1600377.
Hao, R., Yu, D., Sun, Y., Cao, Q., Liu, Y., Liu, Y., 2015. Integrating multiple source data to enhance variation and weaken the blooming effect of DMSP-OLS light. Remote Sens. 7, 1422–1440. https://doi.org/10.3390/rs70201422.
Henderson, J.V., Storeygard, A., Weil, D.N., 2012. Measuring economic growth from outer space. Am. Econ. Rev. 102, 994–1028. https://doi.org/10.1257/aer.102.2.994.
Hu, J., Wang, Y., Ying, Q., Zhang, H., 2014. Spatial and temporal variability of PM2.5 and PM10 over the North China Plain and the Yangtze River Delta, China. Atmos. Environ. 95, 598–607.
Imhoff, M.L., Lawrence, W.T., Stutzer, D.C., Elvidge, C.D., 1997. A technique for using composite DMSP/OLS "city lights" satellite data to map urban area. Remote Sens. Environ. 61, 361–370. https://doi.org/10.1016/S0034-4257(97)00046-1.
Kyba, C., Garz, S., Kuechly, H., de Miguel, A.S., Zamorano, J., Fischer, J., Hölker, F., 2014. High-resolution imagery of earth at night: new sources, opportunities and challenges. Remote Sens. 7 (1), 1–23.
Letu, H., Hara, M., Yagi, H., Naoki, K., Tana, G., Nishio, F., Shuhei, O., 2010. Estimating energy consumption from night-time DMSP/OLS imagery after correcting for saturation effects. Int. J. Remote Sens. 31, 4434–4458.
Letu, H., Hara, M., Tana, G., Bao, Y., Nihio, F., 2015. Generating the nighttime light of the human settlements by identifying periodic components from DMSP/OLS satellite imagery. Environ. Sci. Technol. 49, 10503–10509.
Levin, N., 2017. The impact of seasonal changes on observed nighttime brightness from 2014 to 2015 monthly VIIRS DNB composites. Remote Sens. Environ. 193, 150–164.
Li, X., Zhou, Y., 2017. Urban mapping using DMSP/OLS stable night-time light: a review. Int. J. Remote Sens. 38, 6030–6046. https://doi.org/10.1080/01431161.2016.1274451.
Li, X., Li, D., Xu, H., Wu, C., 2017. Intercalibration between DMSP/OLS and VIIRS night-time light images to evaluate city light dynamics of Syria's major human settlement during Syrian Civil War. Int. J. Remote Sens. 38, 5934–5951.
Liang, S., 2003. Quantitative Remote Sensing of Land Surfaces. John Wiley & Sons, Inc., New Jersey.
Lo, C.P., 2002. Urban indicators of China from DN-calibrated digital DMSP-OLS nighttime images. Ann. Assoc. Am. Geogr. 92, 225–240.
Longcore, T., Rich, C., 2004. Ecological light pollution. Front. Ecol. Environ. 2, 191–198.
Lu, D., Tian, H., Zhou, G., Ge, H., 2008. Regional mapping of human settlements in southeastern China with multisensor remotely sensed data. Remote Sens. Environ. 112, 3668–3679.
National Bureau of Statistics of China, 2014. China City Statistical Yearbook 2014. China Statistics Press, Beijing.
Pandey, B., Zhang, Q., Seto, K., 2017. Comparative evaluation of relative calibration methods for DMSP/OLS nighttime lights. Remote Sens. Environ. 195, 67–78.
Proville, J., Zavala-Araiza, D., Wagner, G., 2017. Night-time lights: a global, long term look at links to socio-economic trends. PLoS One 12 (3), e0174610. https://doi.org/10.1371/journal.pone.0174610.
Richter, R., 1996. A spatially adaptive fast atmospheric correction algorithm. Int. J. Remote Sens. 17 (6), 1201–1214.
Rodrigues, P., Aubrecht, C., Gil, A., Longcore, T., Elvidge, C., 2012. Remote sensing to map influence of light pollution on Cory's shearwater in Sao Miguel Island, Azores Archipelago. Eur. J. Wildl. Res. 58, 147–155.
Rohner, D., Thoenig, M., Zilibotti, F., 2013. Seeds of distrust: conflict in Uganda. J. Econ. Growth 18, 217–252. https://doi.org/10.1007/s10887-013-9093-1.
Small, C., Elvidge, C.D., 2013. Night on Earth: mapping decadal changes of anthropogenic night light in Asia. Int. J. Appl. Earth Obs. Geoinf. 22, 40–52.
Small, C., Pozzi, F., Elvidge, C.D., 2005. Spatial analysis of global urban extent from DMSP-OLS night lights. Remote Sens. Environ. 96, 277–291.
Small, C., Elvidge, C.D., Balk, D., Montgomery, M., 2011. Spatial scaling of stable night lights. Remote Sens. Environ. 115, 269–280. https://doi.org/10.1016/j.rse.2010.08.021.
Townsend, A.C., Bruce, D.A., 2010. The use of night-time lights satellite imagery as a measure of Australia's regional electricity consumption and population distribution. Int. J. Remote Sens. 31 (16), 4459–4480.
van Donkelaar, A., Martin, R.V., Brauer, M., Hsu, N.C., Kahn, R.A., Levy, R.C., Lyapustin, A., Sayer, A.M., Winker, D.M., 2016. Global estimates of fine particulate matter using a combined geophysical-statistical method with information from satellites, models, and monitors. Environ. Sci. Technol. 50, 3762–3772. https://doi.org/10.1021/acs.est.5b05833.
Wang, J., Aegerter, C., Xu, X., Szykman, J.J., 2016. Potential application of VIIRS Day/Night Band for monitoring nighttime surface PM2.5 air quality from space. Atmos. Environ. 124, 55–63.
Xie, Y., Weng, Q., 2017. Spatiotemporally enhancing time-series DMSP/OLS nighttime light imagery for assessing large-scale urban dynamics. ISPRS-J. Photogramm. Remote Sens. 128, 1–15.

Xu, Z., Xia, X., Liu, X., Qian, Z., 2015. Combining DMSP/OLS nighttime light with echo state network for prediction of daily PM2.5 average concentrations in Shanghai, China. Atmosphere 6, 1507–1520. https://doi.org/10.3390/atmos6101507.

Zhang, Q., Schaaf, C., Seto, K.C., 2013. The vegetation adjusted NTL urban index: a new approach to reduce saturation and increase variation in nighttime luminosity. Remote Sens. Environ. 129, 32–41. https://doi.org/10.1016/j.rse.2012.10.022.

Zhang, X., Wu, J., Peng, J., Cao, Q., 2017. The uncertainty of nighttime light data in estimating carbon dioxide emissions in China: a comparison between DMSP-OLS and NPP-VIIRS. Remote Sens. 9 (8), 797. https://doi.org/10.3390/rs9080797.

Zhou, Y., Smith, S.J., Elvidge, C.D., Zhao, K., Thomson, A., Imhoff, M., 2014. A cluster-based method to map urban area from DMSP/OLS nightlights. Remote Sens. Environ. 147, 173–185.

Zhou, Y., Smith, S.J., Zhao, K., Imhoff, M., Thomson, A., Bond-Lamberty, B., Asrar, G.R., Zhang, X., He, C., Elvidge, C.D., 2015. A global map of urban extent from nightlights. Environ. Res. Lett. 10. https://doi.org/10.1088/1748-9326/10/5/054011.

Zhuo, L., Ichinose, T., Zheng, J., Chen, J., Shi, P.J., Li, X., 2009. Modeling the population density of China at the pixel level based on DMSP/OLS non-radiance calibrated nighttime light image. Int. J. Remote Sens. 30 (4), 1003–1018.

Zhuo, L., Zheng, J., Zhang, Z., Li, J., Liu, L., 2015. An improved method of night-time light saturation reduction based on EVI. Int. J. Remote Sens. 36 (16), 4114–4130. https://doi.org/10.1080/01431161.2015.1073861.